Fluid Antenna Systems Enabled by Reconfigurable Holographic Surfaces: Beamforming Design and Experimental Validation

Shupei Zhang, Yuze Zhang, *Graduate Student Member, IEEE,* Hiroaki Hashida, *Member, IEEE,* Yonina C. Eldar, *Fellow, IEEE,* Marco Di Renzo, *Fellow, IEEE,* Boya Di, *Senior Member, IEEE*

***Abstract*—Fluid antenna systems (FASs) have emerged as a promising antenna technology for 6G networks by tapping into new degrees of freedom (DoF) in antenna positions to harness multiplexing gains. In this paper, we propose an implementation of FASs enabled by reconfigurable holographic surfaces (RHSs) and construct a 384-element prototype. Benefiting from its amplitude-modulation capabilities, RHSs can adjust the antenna positions by activating different subsets of elements. However, due to unknown user locations, multiple antenna ports and varying channel environments, beamforming schemes relying on acquiring accurate channel state information (CSI) suffer high complexity. To avoid CSI acquisition, we design a low-overhead fluid beam training scheme for RHS-enabled FAS. Unlike fixed-position antennas, fluid beam training employs different antenna positions via element activation, namely sliding windows, for each codeword to improve the channel quality, thereby enhancing the received signal strength (RSS). Such an element activation method is also applied to reprogram the effective array aperture, hence the fluid beam training adopts a hierarchical structure where the beamwidth of codewords narrows across layers. Experimental and simulation results verify the variation of RSS with sliding windows. Compared to traditional schemes, the proposed fluid beam training utilizing sliding windows achieves higher training accuracy and data rates.**

***Index Terms*—Fluid antenna system, reconfigurable holographic surface, beam training.**

I. Introduction

With the emergence of various intelligent applications, future 6G networks are anticipated to usher in revolutionary changes compared to 5G, targeting enhancements in peak data rates, end-to-end latency and more [1], [2], [3]. In the pursuit of novel antenna technologies to fulfill the 6G benchmarks, fluid antenna system (FAS) is an emerging antenna technology that represents the next generation of reconfigurable antennas [4], [5], [6]. FAS envisions a "formless" antenna featuring a radiating position and/or shape that evolves in a fluid-like manner, enabling the signal to navigate obstacles for reliable connections [7]. The fluid characteristic denotes the capability to dynamically alter the antenna's configuration, which can be realized through the movement of antenna elements, shape modifications using fluidic materials, or reconfiguration via RF-switchable arrays [8], [9], [10]. By exploring new degrees of freedom (DoF) enabled by the antenna positions, FAS can improve the channel conditions to achieve strong channel gains [11], [12], [13].

Benefiting from the amplitude modulation capability, activating elements at specific positions is equivalent to adjusting the antenna positions, thereby rendering reconfigurable holographic surfaces (RHSs) a promising implementation approach for FASs. Specifically, RHS is a type of metamaterial leaky-wave antenna, where electromagnetic (EM) waves are fed into the surface and sequentially excite each element along the surface [14]. By regulating the amplitude of each element through simple diode circuits, the EM waves radiated by each element are superimposed into a directional beam using holographic principles [15]. Unlike traditional parallel-fed phased arrays where the element responses are assumed independent [16], the RHS operates as a series-fed leaky-wave antenna, and the radiated energy of adjacent elements is mutually coupled. Radiating element selection in RHS-enabled FASs requires considering variations in the energy and phase of the EM waves as they propagate on the metasurface, i.e., the positions of activated elements have an effect on the radiation pattern.

Despite the capability of RHS-enabled FAS to enhance the channel gain by adjusting the positions of its elements, the channel from the user to FAS is intricate due to the unknown user locations and scatterers in the environment [17]. As the antenna position changes, traditional pilot-based channel estimation schemes encounter high complexity. Beam training emerges as a practical beamforming solution that circumvents the need for accurate channel state information (CSI) acquisition methods [18]. Specifically, the codebook is first designed, containing multiple codewords for configuring the beamformer. Each codeword corresponds to a beamformer that generates a beam in a specific direction. Beam training is then conducted by traversing all codewords to find the optimal beamformer that aligns with the user channel and maximizes the received signal strength [19].

Existing works on transmission schemes for FASs mainly focus on beamforming methods that assume perfect CSI [20] - [22] or rely on pilot-based channel estimation methods [23] - [25]. In [20], a joint optimization scheme for the transmit beamformer at the BS and the antenna position of FAS at the user side is designed to maximize energy efficiency given near-field CSI. In [21], an FAS-aided simultaneous wireless information and power transfer system is studied, and an

Shupei Zhang, Yuze Zhang, and Boya Di are with State Key Laboratory of Advanced Optical Communication Systems and Networks, School of Electronics, Peking University, Beijing, China (email: zhangshupei@pku.edu.cn; yuze.zhang@stu.pku.edu.cn; diboya@pku.edu.cn).

H. Hashida is with Frontier Research Institute for Interdisciplinary Sciences, Tohoku University, Sendai, Japan (email: hiroaki.hashida.d6@tohoku.ac.jp).

Yonina C. Eldar is with the Faculty of Mathematics and Computer Science, Weizmann Institute of Science, Rehovot 7610001, Israel (email: yonina.eldar@weizmann.ac.il).

M. Di Renzo is with Université Paris-Saclay, CNRS, CentraleSupélec, Laboratoire des Signaux et Systèmes, 3 Rue Joliot-Curie, 91192 Gif-sur-Yvette, France (email: marco.di-renzo@universite-paris-saclay.fr), and with King's College London, Centre for Telecommunications Research – Department of Engineering, WC2R 2LS London, United Kingdom (email: marco.di_renzo@kcl.ac.uk).

alternating optimization approach is proposed to maximize the communication rate while satisfying the power requirements. In [23], channel estimation and reconstruction aspects for FASs are investigated using Nyquist sampling and maximum likelihood estimation methods. Leveraging the sparsity of the channel, the scheme proposed in [24] estimates the channel by selectively switching each fluid antenna among a limited set of estimated positions.

However, the existing works did not address the design of beam training schemes for FASs. To circumvent the acquisition of CSI for beamforming, it is necessary to devise a low-overhead beam training scheme for FASs by leveraging the adaptability of the antenna positions. Benefiting from the amplitude-modulation capability of its reconfigurable elements, RHS provides a feasible approach to realize antenna repositioning. Specifically, modulating the radiation amplitude of the elements at specific locations on the RHS for activating and deactivating them is equivalent to adjusting the aperture and position of the antennas in RHS-enabled FAS.

In this paper, we propose a low-overhead beam training scheme for RHS-enabled FAS, where both codeword design and beam training leverage the DoF in antenna positions to enhance the strength of the received signal. An amplitude modulation method for RHS is presented to equivalently adjust the array aperture and positions of the FAS elements, i.e., elements at specific locations are selectively activated. By employing various equivalent apertures, codewords with varying beam coverage are designed to support hierarchical beam training. During beam training, for each equivalent array aperture of different sizes, different sets of elements are activated, forming a *sliding window* moving along the surface of the RHS. The contributions of this paper are summarized as follows:

1) We propose an approach to implement the FAS utilizing an RHS, where the array aperture and positions of the RHS elements can be reconfigured via amplitude modulation. The received signal strength by controlling the amplitude responses of the elements is analyzed theoretically. Experiments based on an RHS prototype are presented to demonstrate that the received signals can be enhanced by activating or deactivating elements at specific locations.
2) Benefiting from the amplitude-modulation capability of RHS, an RHS array reconfiguration method is presented to change the equivalent array aperture by activating or deactivating elements at specific locations. Moreover, by manipulating the equivalent array aperture, codeword designs for different beam coverage are proposed.
3) A fluid beam training scheme is proposed utilizing different sliding windows of RHS-enabled FASs. In beam training, a codeword could correspond to multiple sliding windows. The channel conditions are improved by adjusting the position of the sliding window, thereby enhancing the received signal strength and beam training accuracy.
4) By developing a hardware testbed for RHSs, the effectiveness of the proposed codeword design and fluid beam training scheme is validated experimentally. It is shown that the use of sliding windows for beam training improves the accuracy of beam training and data rate.

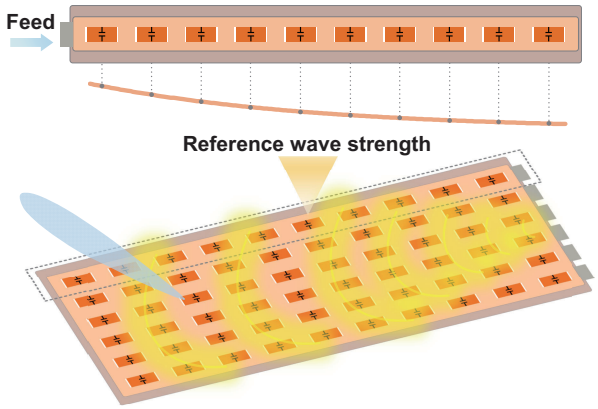

Fig. 1. RHS schematic diagram.

Organization: The rest of this paper is organized as follows. In Section II, the RHS model, RHS-enabled FAS, and the signal model are introduced. Key Ideas of RHS-enabled FAS including the aperture-changeable array and the sliding window are presented in Section III. The hierarchical codebook design based on the aperture-changeable RHS is proposed in Section IV. We design the fluid beam training scheme using the sliding windows approach in Section V. The experimental results and simulation results are presented in Section VI and Section VII, respectively. Conclusions are drawn in Section VIII.

Notation: The unbolded symbol a represents a scalar, the lowercase bolded symbol $\mathbf{b}$ denotes a vector, and an uppercase bolded letter $\mathbf{B}$ represents a matrix. A script letter $\mathcal{B}$ is used to represent a set. $[\mathbf{B}]_{m,n}$ represents the element at the n-th column of the m-th row in the matrix, and $\mathbf{B}^H$ represents the conjugate transpose of a matrix. The real and imaginary parts of a complex number a are denoted as $\mathrm{Re}(a)$ and $\mathrm{Im}(a)$, respectively. The modulus of a complex number a is denoted as $|a|$. The operator $\odot$ represents the Hadamard product.

II. System Model and Problem Formulation

In this section, we introduce the working principle of RHS, the idea of RHS-enabled FAS, and the signal model. Then the problem of codebook-based beam training for FASs is formulated.

A. RHS Model

RHS is a type of serial leaky-wave array composed of feeds and a number of densely packed metamaterial radiated elements. As shown in Fig. 1 where the element structure of one-dimensional and two-dimensional RHS is identical, the feed delivers the input signal into EM waves, referred to as the reference wave. The RHS employs a series-fed approach, where the reference wave propagates along the metasurface and sequentially excites the RHS elements. The reference wave transforms into leaky waves through the slot structures of the RHS elements, radiating energy into free space [27].

The radiation amplitude of the radiated wave at each element can be individually adjusted to enable directional

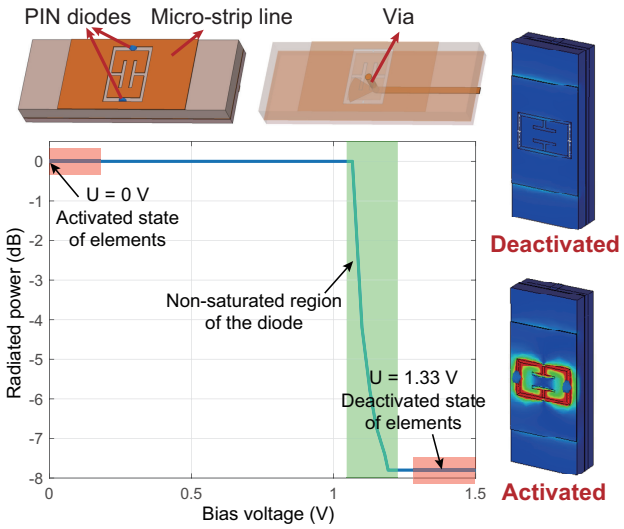

Fig. 2. RHS element structure (top), electric field strength of activated and deactivated elements (right), and element radiated power with diode bias voltage.

holographic beamforming, implemented through a complementary electric-LC (cELC) resonator loaded as shown in Fig. 2. The cELC resonator comprises a microstrip line etched with a circle of annular slot, incorporating two PIN diodes that are connected across the gaps separating the micro-strip line from the central metal patch. By modulating the bias voltage applied to these diodes, their conductive states can be switched between ON and OFF states. The states of the diodes determine both the mutual inductance of the cELC resonator and the element radiation state [26]. The electric field strength of RHS elements in activated and deactivated states is shown in Fig. 2. In practice, bias voltages of 0 V and 1.33 V are applied to activate and deactivate the RHS element, respectively.

Assuming that RHS consists of N elements and L feeds, we denote the distance from the l-th feed to the n-th element as $\mathbf{r}_{l,n}$. Considering the propagation loss along RHS, the response of the l-th feed at the n-th element is expressed as $e^{-\alpha|\mathbf{r}_{l,n}|} \cdot e^{-j\mathbf{k}_s \cdot \mathbf{r}_{l,n}}$, where α represents the propagation loss factor, and $\mathbf{k}_s$ denotes the wavenumber vector on RHS. The normalized radiation amplitude m_n of the n-th element is adjusted by the diode-based controllers. Considering the responses from all feeds, the n-th element of the RHS holographic beamformer $\mathbf{v} \in \mathbb{C}^{N\times 1}$ is given by [15], [27]

$$v_n = \sum_{l=1}^{L} \sqrt{\eta} \cdot m_n \cdot e^{-\alpha|\mathbf{r}_{l,n}|} \cdot e^{-j\mathbf{k}_s \cdot \mathbf{r}_{l,n}}, \tag{1}$$

where η represents the ratio of the power received by each element to the total power of the reference wave emitted from the feeds. Define $\mathbf{m} = [m_1, \cdots, m_N]$ as the amplitude vector, the directional holographic beam can be generated by adjusting $\mathbf{m}$ [28].

B. Description of RHS-Enabled FAS

Consider a downlink wireless communication system. To improve the channel quality during transmission, the base station (BS) is equipped with RHS-enabled fluid antennas to serve a single-antenna user[1]. Analog beamforming is achieved at the RHS by controlling the radiation amplitude of each element, i.e., m_n [28]. Benefiting from the amplitude-modulation characteristics of RHS, the number and positions of selected antennas can be changed by RHS-enabled FAS. Specifically, as shown in Fig. 3, we consider a one-dimensional RHS equipped with N elements and a feed. Here, we employ a one-dimensional RHS to facilitate the mathematical formulation, which can be easily extended to the two-dimensional case, as shown in Sections VI and Sec-VII. The BS initially up-converts the signal to the carrier frequency through the RF chain and then sends the signal into the RHS via the feed.

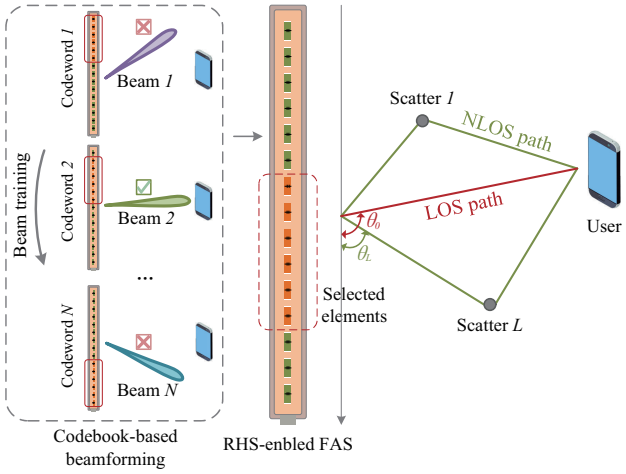

Fig. 3. RHS-enabled FAS aided communications.

C. Signal Model

The user channel consists of both line-of-sight (LOS) and non-line-of-sight (NLOS) paths. Assume that there are L NLOS paths, each corresponding to a scatterer, the angle of arrival (AoA) of the l-th scatterer relative to the BS is θ_l. The AoA of the user, i.e., the LOS path, is θ_0. According to the multi-ray channel model, the channel $\mathbf{h} \in \mathbb{C}^{1\times N}$ between the user and the BS can be expressed as [29]

$$\mathbf{h} = \sqrt{\frac{\kappa N}{\kappa+1}} e^{j\omega_0} \mathbf{b}(\psi_0) + \sqrt{\frac{N}{L}} \sum_{l=1}^{L} \beta_l \mathbf{b}(\psi_l), \tag{2}$$

where $\psi_o = \cos(\theta_0)$ and $\psi_l = \cos(\theta_l)$. Also, κ is the Rician factor representing the ratio of power between the LOS and the NLOS paths, and ω_0 is the random phase of the LOS component. The complex gain β_l of the NLOS path follows $\beta_l \sim \mathcal{CN}(0, \sigma_{\beta,l}^2)$ where $\sigma_{\beta,l}^2 = 1/\kappa + 1$. The steering vector $\mathbf{b}(\psi) \in \mathbb{C}^{1\times N}$ is defined as [30], [31]

$$\mathbf{b}(\psi) = \frac{1}{\sqrt{N}} \left[1, e^{-j\frac{2\pi}{\lambda}d\psi}, \cdots, e^{-j\frac{2\pi}{\lambda}d(N-1)\psi}\right], \tag{3}$$

where d is the antenna spacing and λ is the wavelength.

Assume the symbol transmitted to the user is s, after beamforming through RHS-enabled FAS, the signal received by the user is given by

$$y = \mathbf{h}\mathbf{v}s + n, \tag{4}$$

[1]This scheme can be extended to multi-user beam training scenarios, which requires high-resolution amplitude modulation of RHS elements.

where $|s|^2 = 1$, and $n \sim \mathcal{CN}\left(0, \sigma^2\right)$ is the white Gaussian noise.

D. FAS-Aided Codebook-Based Transmission Scheme

To circumvent the acquisition of CSI which entails high complexity due to unknown user locations, multiple antenna ports, and varying channel environments, this paper considers a practical beamforming scheme based on codebook design and beam training. The codebook $\mathcal{V}$ for RHS-enabled FAS consists of multiple codewords. Each codeword $\mathbf{v}$ corresponds to an amplitude vector $\mathbf{m}$ of the RHS elements, and can generate a beam in a specific direction. As illustrated in Fig. 3, the objective of beam training is to sequentially configure the RHS with each codeword to transmit signals, then select the optimal codeword that maximizes the received signal strength based on user feedback [18].

Unlike traditional fixed-position antenna schemes, the proposed approach leverages the amplitude-modulation capability of RHS to generate codewords with varying beamwidths by adjusting the equivalent aperture of the array. This method narrows the search range for user channel angles, as detailed in Section IV. Moreover, the RHS-enabled FAS can dynamically adjust the array position during beam training to improve channel quality and enhance received signal strength, which is elaborated in Section V.

The received signal is jointly determined by the user channel, the propagation of EM waves on the RHS, and the position and number of activated elements. To maximize the received signal strength through FAS-based codebook design and beam training, the problem can be formulated as

$$\max_{\mathbf{m},M,Q} \quad |\mathbf{h}\mathbf{v}(\mathbf{m}, M, Q)|^2 \tag{5a}$$

$$\text{s.t. } \mathbf{v}(\mathbf{m}, M, Q) \in \mathcal{V}, \tag{5b}$$

$$M \in \{1, 2, \cdots, N\}, \tag{5c}$$

$$m_n = 0, n<Q \text{ and } n>M+Q-1, \tag{5d}$$

$$m_n = 0 \text{ or } 1, \quad \forall n, \tag{5e}$$

where constraint (5b) indicates that the holographic beamformer $\mathbf{v}$ in beam training is configured based on codewords from the pre-designed codebook $\mathcal{V}$. Constraint (5c) specifies the range of the equivalent aperture M, i.e., the number of selected elements, in the codeword design. Constraint (5d) indicates that, during beam training, for a given equivalent aperture M and array position Q, the elements not selected in the equivalent array are deactivated as shown in Fig 5. Constraint (5e) represents the finite amplitude values of RHS elements. Here we consider 1-bit amplitude modulation, which proves sufficient for single-user communication [26]. Considering hardware constraints and design complexity, practical RHS implementations often employ 1-bit amplitude modulation [15].

Note that traditional subarray selection schemes for phased arrays cannot address Problem (5) directly [16], [32], where the responses of the elements are mutually independent. For RHS-enabled FAS that operates as a series-fed leaky-wave antenna, the energy and phase of EM waves vary with the position of the elements as they propagate along the RHS surface. This brings a coupling of energy between elements, making their radiation responses no longer independent. Based on the holographic principle, antenna selection in RHS requires considering the superposition of EM waves radiated by the elements in the equivalent array to form directional beams. Therefore, a dedicated antenna selection scheme for RHS-enabled FAS is necessary.

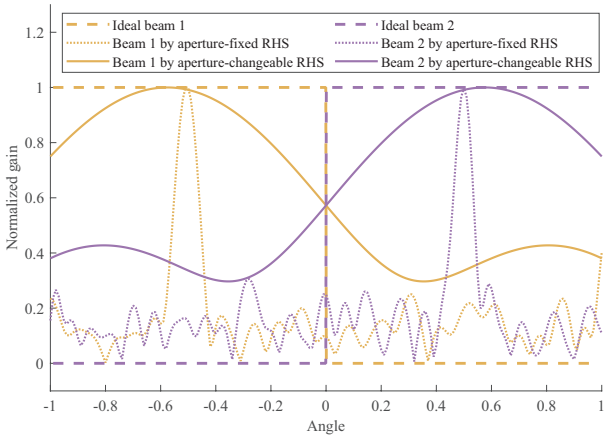

Fig. 4. Ideal and practical beam patterns of 1-bit aperture-fixed RHS.

III. Motivation for RHS-Enabled FAS

In this section, we start with the limitations of traditional aperture-fixed arrays in beam design given practical finite-resolution constraints. The solution concept of aperture-changeable RHS arrays is then introduced. It provides different efficient apertures at various positions, forming multiple *sliding windows*. Finally, we highlight that the signal varies with the position of sliding windows, which could enhance the signal strength in the beam training.

A. Limitations of Aperture-Fixed Arrays

According to antenna theory, the beamwidth generated by an antenna array is determined by the array aperture, expressed as [33]

$$B_N = \frac{\lambda}{D}, \tag{6}$$

where D represents the antenna aperture. For a uniform linear array, $D = Nd$, where d is the element spacing.

To avoid the high complexity of exhaustive beam training, codewords with varying beam coverages are able to narrow the search range, thereby reducing training overhead. For an aperture-fixed antenna array, designing beams with different coverages necessitates each antenna element to be high-precision controlled [34], i.e., through high-resolution phase shifters for phased arrays and the continuous amplitude responses for RHSs. A low resolution of the antenna elements may result in a discrepancy between the practical beam pattern and the ideal beam pattern, making it impractical to match user channels during beam training. This is because, in the beam design, the theoretically optimal values of antenna configuration deviate greatly from the available finite values.

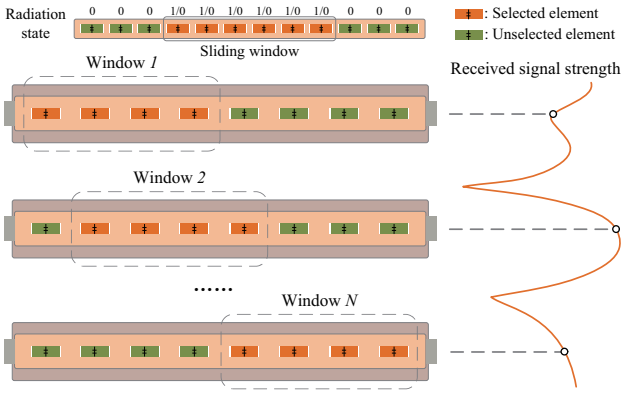

Fig. 5. Aperture-changeable RHS array with sliding windows. Within a window, each RHS element is activated or deactivated. The channel varies with the window position, consequently affecting the received signal strength of the user.

Due to hardware constraints and design complexity, practical antenna elements typically operate with limited resolutions. For instance, common RHS prototypes employ 1-bit amplitude modulation [15]. Fig. 4 shows the beams designed using a 64-element RHS. The expected beam coverage spans 90 90° (indicated by dashed lines), whereas the beam coverage generated using the 1-bit aperture-fixed RHS measures only 9° (indicated by dotted lines). This is because due to the excessively narrow beamwidth dictated by the array aperture in (6), the practical beam patterns fail to cover the desired angles. It thus necessitates an aperture-changeable method.

B. Aperture-Changeable RHS Array with the Sliding Window

Since the beamwidth is related to the array aperture, leveraging the amplitude-modulation characteristics of RHSs, different beam widths can be obtained by adjusting the equivalent aperture of the array without increasing the resolution of amplitude responses. Specifically, RHS elements with an amplitude of 0, due to their absence of EM wave radiation, are considered to be in a turned-off state. By modulating the element amplitude to deactivate or activate RHS elements at specific positions, the equivalent aperture of the array is changed [35].

As indicated by (6), the beamwidth is inversely proportional to the array aperture. When generating a wide beam, the equivalent aperture of the array is reduced by sequentially deactivating RHS elements. Conversely, to generate a narrow beam, RHS elements are sequentially selected. As shown in Fig. 4, even for 1-bit amplitude modulation, the beamwidth can be adjusted by adjusting the equivalent aperture of the array. Notably, this method requires no additional switch circuits or mechanisms.

As illustrated in Fig. 5, when designing beams by adjusting the equivalent aperture of the RHS array, the position of the equivalent array is not unique. Leveraging the amplitude-modulation characteristics of RHS elements, multiple arrays with identical equivalent apertures, i.e., sliding windows, can be generated along the RHS. The amplitude responses of elements outside the window are set to zero to deactivate them, while those within the window are adjustable.

Remark 1. *As shown in Fig.5, if the number of elements in the equivalent array is M, there are $(N-M+1)$ possible sliding windows, which increases the degrees of freedom in beam design.*

C. Signal Strength Varying with Sliding Window Positions

To adjust the equivalent array aperture, based on **Remark** 1, the antenna position can also be exploited by changing the window location of the array along the surface. Assume the number of selected elements is M and the position of the first selected element is Q, the antenna state vector $\mathbf{u} \in \mathbb{C}^{1\times N}$ is defined as

$$\mathbf{u}(M,Q) = [0,\cdots,0,1_Q,\cdots,1_{Q+M-1},0,\cdots,0]. \tag{7}$$

Hence, the equivalent channel $\widetilde{\mathbf{h}} \in \mathbb{C}^{1\times N}$ and steering vector $\widetilde{\mathbf{b}} \in \mathbb{C}^{1\times M}$ can be expressed as

$$\widetilde{\mathbf{h}}(M,Q) = \mathbf{h} \odot \mathbf{u}(M,Q), \tag{8}$$

$$\widetilde{\mathbf{b}}(\psi,M,Q) = \mathbf{b}(\psi) \odot \mathbf{u}(M,Q). \tag{9}$$

In the beam training, the codewords are designed based on the steering vector of the LOS path, since NLOS paths are random. Assume the user's angle is ψ_0 and the number of selected elements in RHS-enabled FAS is M, the optimal beamformer under the transmit power constraint is $\mathbf{v}^* = \frac{\widetilde{\mathbf{b}}(\psi_0,M,Q)^H}{|\widetilde{\mathbf{b}}(\psi_0,M,Q)^H|}$. In this case, the received signal strength of the user varies with the sliding window position, denoted as

$$\begin{aligned}
&|y(Q) = |\widetilde{\mathbf{h}}(M,Q)\mathbf{v}^* + n| \\
=&|(\sqrt{\frac{\kappa N}{\kappa+1}}e^{j\omega_0}\widetilde{\mathbf{b}}(\psi_0,M,Q) + \sqrt{\frac{N}{L}}\sum_{l=1}^{L}\beta_l\widetilde{\mathbf{b}}(\psi_l,M,Q))\mathbf{v}^* + n| \\
=&|\sqrt{\frac{\kappa M}{\kappa+1}}e^{j\omega_0} + \sqrt{\frac{1}{LM}}\sum_{l=1}^{L}\beta_l\sum_{n=Q}^{Q+M-1}e^{j\frac{2\pi}{\lambda}(n-1)d\Delta_l} + n| \\
=&|\underbrace{\sqrt{\frac{\kappa M}{\kappa+1}}e^{j\omega_0}}_{LOS} + \underbrace{\sqrt{\frac{1}{LM}}\sum_{l=1}^{L}\beta_l\frac{e^{j\frac{2\pi}{\lambda}(Q-1)d\Delta_l}(1-e^{j\frac{2\pi}{\lambda}Md\Delta_l})}{1-e^{j\frac{2\pi}{\lambda}d\Delta_l}}}_{NLOS} + n|,
\end{aligned} \tag{10}$$

where $\Delta_l = \cos\psi_l - \cos\psi_0$. As the position of the window changes, the primary factor influencing the received signal strength comes from the NLOS paths. For the l-th path, the signal strength exhibits periodic variations as the window position changes, where the periodicity is $T_l = \lambda/d\Delta_l$.

Case 1: When the number of NLOS paths is $L = 1$, the signal strength $|y(Q)|$ is periodic with a period $T = \frac{\lambda}{d\Delta_1}$. During the window sliding process, there are at most $\lfloor\frac{N-M+1}{T}\rfloor + 1$ optimal positions where high signal strength occurs.

Case 2: When the number of NLOS paths is $L > 1$, the signal strength $|y(Q)|$ is periodic with a period T, where T is the least common multiple of $[T_1,\cdots,T_L]$. During the window sliding process, there are at most $\lfloor\frac{N-M+1}{T}\rfloor + 1$ optimal positions where high signal strength occurs.

Fig. 6 shows the variation of the received signal strength with window position given different window sizes, numbers of NLOS paths, and NLOS path intensities. Signal envelopes are observed across various window sizes. When the number of paths is $L = 1$ as **Case 1**, the signal strength changes

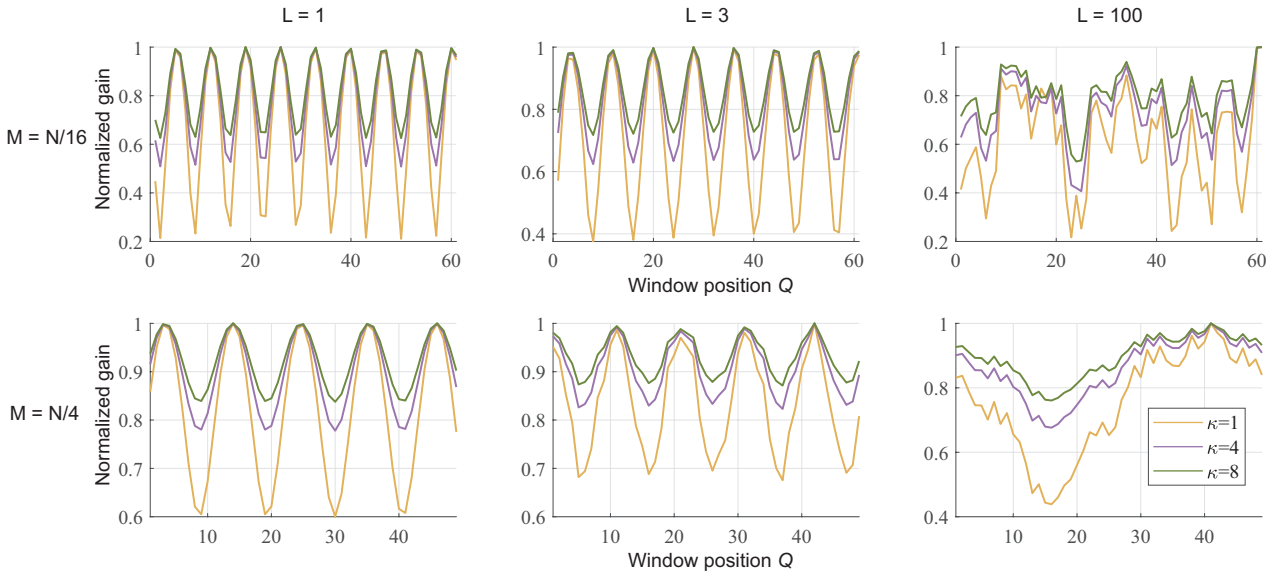

Fig. 6. Signal strength influenced by the window position, where L represents the number of NLOS path, M is the window size, and $kappa$ is the Rician factor.

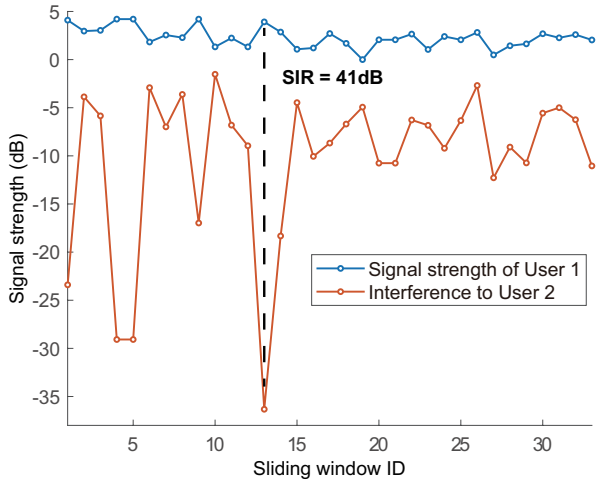

Fig. 7. SIR influenced by the window position.

periodically with the window position, where the period is related to the angles of the LOS and NLOS paths. As the number of paths increases, the periodicity of signal strength becomes longer. Within a given number of sliding windows, the signal strength exhibits irregularity as **Case 2**. When the Rician factor κ increases, indicating an increase in the intensity of the LOS path, the degree of variation in signal strength with window position decreases.

Remark 2. *Since beam training relies on the user's received signal strength, adjusting the window position of the equivalent array during beam training can enhance the signal strength, thereby improving the accuracy of beam training.*

In multi-user systems, the RHS-enabled FAS can not only enhance the received signal strength for target users through window positioning but also simultaneously suppress interference to other users. As illustrated in Fig. 7, when the RHS-enabled FAS beam aligns with User 1, we define the signal-to-interference ratio (SIR) as the ratio of User 1's received strength to the interference caused to User 2. It is observed that the maximum SIR can reach 41 dB through window positioning, demonstrating the capability of RHS-enabled FAS to enhance signal strength while suppressing interference.

IV. Hierarchical Codebook Design of Aperture-Changeable RHS

This section first introduces the design objectives of beam training and the hierarchical codebook structure. After that, the details of the multi-resolution codeword and hierarchical codebook design are presented.

A. Characteristics of Beam Training for RHS-enabled FAS

To solve (5) given the finite adjustable amplitude values of the RHS, as well as the changeable array aperture nature, the characteristics of beam training for RHS-enabled FAS are listed as follows:

- **Low Training Overhead:** The overhead of traditional exhaustive beam training scales linearly with the number of antenna elements, depleting the effective transmission time. RHS-enabled beam training is expected to search for the user direction by designing codewords with varying coverage resolutions, thereby reducing the overhead to a logarithmic scale with the number of antenna elements.
- **Aperture-Changeable Array:** As discussed in Section III-A, for traditional aperture-fixed arrays, designing codewords with varying beam coverage is challenging due to limited element resolution. Leveraging the amplitude-modulation characteristics of RHS, the beamwidth can be controlled by adjusting the equivalent array aperture, even for only 1-bit amplitude resolution.
- **Selective Sliding Windows:** In traditional beam training, the channel quality remains unchanged due to the fixed

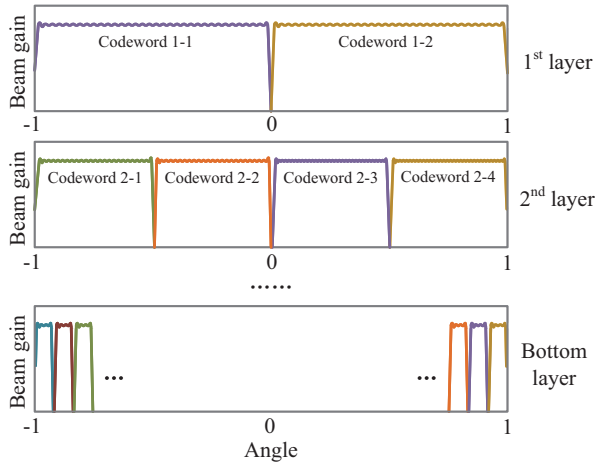

Fig. 8. Hierarchical structure of the RHS codebook.

positions of the array. As analyzed in Section III-C, the channel quality can be optimized during the beam training by changing the position of the window, thereby enhancing the received signal strength.

B. Codebook Structure for RHS-enabled FAS

To mitigate the high overhead of the exhaustive beam training, the RHS codebook is designed as a hierarchical structure as depicted in Fig. 8. The codebook comprises S layers, where the s-th layer contains 2^s codewords. The coverage of codewords in the angular domain decreases layer by layer. The codeword in the s-th layer is divided into two codewords in the $s+1$-th layer by splitting its coverage range. As the minimum beamwidth at the bottom level is limited by the array aperture, the number of layers in the codebook satisfies the following constraint

$$S \leq \lfloor \log_2 \frac{2D}{\lambda} \rfloor, \tag{11}$$

where D is the array aperture of RHS.

Denoting the p-th codeword in the s-th layer by $\mathbf{v}_{s,p}$, its beam coverage $\mathbb{P}(\mathbf{v}_{s,p})$ is defined as

$$\mathbb{P}(\mathbf{v}_{s,p}) = \{\, \psi \,|\, |\mathbf{b}(\psi)\mathbf{v}_{s,p}| > |\mathbf{b}(\psi)\mathbf{v}_{s,p'}|, \forall p' \neq p \,\}. \tag{12}$$

As shown in Fig. 8, the coverage $\mathbb{P}(\mathbf{v}^*_{s,p})$ of the ideal codeword $\mathbf{v}^*_{s,p}$ in the angular domain is

$$\mathbb{P}(\mathbf{v}^*_{s,p}) = [\frac{p-1}{2^{s-1}}, \frac{p}{2^{s-1}}]. \tag{13}$$

Benefiting from the hierarchical codebook structure, only two codewords per level are required in the beam training to progressively narrow down the user's potential angles.

C. Codeword Design by Aperture-Changeable RHS

Since the beamwidth is correlated with the equivalent RHS array aperture, we design codewords with different beamwidths by adjusting the equivalent array of the RHS. Moreover, for a specific array aperture, there exist multiple sliding windows, implying that each codeword in Fig. 8 can correspond to different array positions. This provides the potential to enhance channel conditions during beam training.

Designing codewords utilizing the aperture-changeable RHS array can be divided into three steps: 1) Determine the array aperture based on the coverage area of the codewords in each layer. 2) Adjust the amplitude of each element within the window to steer the beam at the desired angles. 3) Select a set of candidate window positions based on codeword gain. We elaborate on each step in detail.

Step 1: For the codewords at the s-th layer, it can be deduced from (13) that the beamwidths of the codewords are all $\frac{1}{2^{s-1}}$. Combining this with the relationship between beamwidth and array aperture given in (6), the equivalent array aperture corresponding to the s-th layer, i.e., the number of selected elements, can be obtained as

$$N_s = \lfloor \frac{\lambda}{d} \rfloor 2^{s-1}. \tag{14}$$

Step 2: As **Remark** 1, for the p-th codeword $\mathbf{v}_{s,p}$ at the s-th layer, there are $(N - N_s + 1)$ possible window positions, and the q-th window corresponds to a unique codeword $\mathbf{v}_{s,p,q}$. The objective of codeword design is to tailor the beam coverage. After **Step 1**, the beamwidth meets the requirement, and the amplitudes of RHS elements within the q-th window are then adjusted to maximize the codeword gain. By jointly considering EM wave propagation on the RHS, window size, and the activation states of elements within the window, the problem can be formulated as

$$\begin{aligned} \max_{\mathbf{v}} \; & |\widetilde{\mathbf{b}}(\psi_{s,p}, N_s, q)\mathbf{v}| \\ \text{s.t.} \; & m_n = 0, n<q \text{ and } n>N_s+q-1 \\ & m_n = 0 \text{ or } 1, \quad \forall n. \end{aligned} \tag{15}$$

We rewrite the RHS beamformer as $\mathbf{v} = [\gamma_1 m_1, \cdots, \gamma_N m_N]$ where $\gamma_n = \sum_{l=1}^{L} \sqrt{\eta} \cdot e^{-\alpha|\mathbf{r}_{l,n}|} \cdot e^{-j\mathbf{k}_s \cdot \mathbf{r}_{l,n}}$, and the maximization problem can be equivalently formulated as

$$\begin{aligned} & |\widetilde{\mathbf{b}}(\psi_{s,p}, N_s, q)\mathbf{v}|^2 \\ =& \mathbf{v}^H \widetilde{\mathbf{b}}(\psi_{s,p}, N_s, q)^H \widetilde{\mathbf{b}}(\psi_{s,p}, N_s, q)\mathbf{v} \\ =& \sum_{n_1=q}^{q+N_s-1} \sum_{n_2=q}^{q+N_s-1} \gamma_{n_1}^H \gamma_{n_2} m_{n_1} m_{n_2} [\mathbf{B}]_{n_1,n_2}, \end{aligned} \tag{16}$$

where $\mathbf{B} = \widetilde{\mathbf{b}}(\psi_{s,p}, N_s, q)^H \widetilde{\mathbf{b}}(\psi_{s,p}, N_s, q)$. For the n-th element, when the amplitudes of other elements are fixed, this equation becomes a quadratic function of m_n, denoted as

$$\begin{aligned} & |\widetilde{\mathbf{b}}(\psi_{s,p}, N_s, q)\mathbf{v}|^2 \\ =& a_{s,p,n} m_n^2 + b_{s,p,n} m_n + c_{s,p,n}, \end{aligned} \tag{17}$$

where the coefficients $a_{s,p,n}$, $b_{s,p,n}$, and $c_{s,p,n}$ of this quadratic function are represented as

$$\begin{aligned} a_{s,p,n} &= |\gamma_n|^2 [\mathbf{B}]_{n,n} \\ b_{s,p,n} &= 2\text{Re}\{ \sum_{n'=q, n' \neq n}^{q+N_s-1} \gamma_n^H \gamma_{n'} [\mathbf{B}]_{n,n'} m_{n'} \} \\ c_{s,p,n} &= 2\text{Re}\{ \sum_{n_1=q, n_1 \neq n}^{q+N_s-1} \sum_{n_2=q}^{q+N_s-1} \gamma_{n_1}^H \gamma_{n_2} m_{n_1} m_{n_2} [\mathbf{B}]_{n_1,n_2} \}. \end{aligned} \tag{18}$$

Algorithm 1: RHS Hierarchical Codebook Design

Input: The layer S of the codebook, initial RHS holographic beamformer $\mathbf{v}$

for $s = 1 : S$ **do**
  for $p = 1 : 2^s$ **do**
    for $q = 1 : N - N_s + 1$ **do**
      Calculate the desired codeword coverage $\mathbb{P}(\mathbf{v}_{s,p}^*)$ according to (13)
      Generate the codeword $\mathbf{v}_{s,p,q}$ through **Step 1,2,3** in Secion IV-C
      Evaluate the codeword gain by $f(q, \mathbf{v}_{s,p,q})$ in (19)
    end
    Arrange the codewords in descending order of $f(q, \mathbf{v}_{s,p,q})$ for each codeword $\mathbf{v}_{s,p}$
  end
end

Output: The RHS hierarchical codebook $\mathcal{V}$.

Algorithm 2: Fluid Beam Training Mechanism

Input: Codebook $\mathcal{V}$, user channel $\mathbf{h}$, and the number of used windows Z

for $s = 1 : S$ **do**
  for $p = 1 : 2$ **do**
    for $q = 1 : Z$ **do**
      Transmitting signals using codeword $\mathbf{v}_{s,2\xi_s-2+p,q}$
      User recodes the signal strength $|y| = |\mathbf{h}\mathbf{v}_{s,2\xi_s-2+p,q}s + n|$
    end
    User recodes the highest signal strength of codeword $\mathbf{v}_{s,2\xi_s-2+p}$
  end
  User feeds back the index τ_s of the codeword with the higher strength
  Update $\xi_s = 2(\xi_{s-1} - 1) + \tau_s$
end

Output: The optimal codeword $\mathbf{v}_{S,\xi_S}$.

Since $[\mathbf{B}]_{n,n} > 0$, the coefficient $a_{s,p,n}$ of the quadratic term is also greater than 0. For a convex quadratic function, when m_n is within the interval $[0, 1]$, the maximum value is always attained at either $m_n = 0$ or $m_n = 1$. Therefore, codewords can be designed by iteratively optimizing the amplitude of each element to maximize the beamforming gain in (15). Moreover, the optimal amplitude values are achieved at either 0 or 1, indicating that 1-bit amplitude modulation is sufficient.

Proposition 1. *In the design of codewords for the aperture-changeable RHS, the optimal amplitude values are attained at either 0 or 1.*

Proof. See **Step 2**. □

Step 3: After the first two steps, the codeword according to an equivalent array aperture of N_s, the window position of q, and the target angle of $\psi_{s,p}$ is designed. We define the p-th codeword in the s-th layer using the window position of q as $\mathbf{v}_{s,p,q}$. As mentioned in **Remark** 1, for codeword $\mathbf{v}_{s,p}$ in Fig. 8, there are $N - N_s + 1$ selectable codewords $\mathbf{v}_{s,p,q}$ in total. As presented in **Remark** 2, to exploit the DoF offered by array positions during beam training, multiple candidate window positions need to be selected for a codeword with the same desired beam coverage. Both the practical coverage and beam gain of a codeword vary with the window position, hence we employ the following function to evaluate the impact of the window position on the designed codeword.

$$\begin{aligned} f(q, \mathbf{v}_{s,p,q}) &= \sum_{i=1}^{I} (|\widetilde{\mathbf{b}}(\psi_i, N_s, q)\mathbf{v}_{s,p,q}| - G_i)^2 \\ \mathbf{s.t.} \quad G_i &= \begin{cases} \epsilon, & \text{if } \psi_i \in \mathbb{P}(\mathbf{v}_{s,p}^*), \\ 0, & \text{else.} \end{cases} \end{aligned} \tag{19}$$

where ϵ is a constant that represents the ideal beam gain of the codeword, and $\mathbb{P}(\mathbf{v}_{s,p}^*)$ denotes the ideal angular coverage of the codeword $\mathbf{v}_{s,p}^*$ as defined in (13). In the angular domain $\psi \in [-1, 1]$, I angles are uniformly sampled, where $\psi_i = -1 + \frac{2i-1}{I}$. It is expected that the beam gain within the ideal coverage of the codeword is ϵ, while the beam gain outside the coverage is 0. That is, a smaller value of the evaluation function in (19) implies that the codeword at this window position is closer to the ideal codeword. The sequence numbers of the $N - N_s + 1$ windows are then sorted based on codeword gain as $[q_1, \cdots, q_{N-N_s+1}]$, where $f(q_1, \mathbf{v}_{s,p,q_1}) < \cdots < f(q_{N-N_s+1}, \mathbf{v}_{s,p,q_{N-N_s+1}})$.

By designing codewords for all possible windows layer by layer, the design of the hierarchical codebook $\mathcal{V}$ is summarized in **Algorithm** 1. The codebook design exhibits a computational complexity of $\mathcal{O}(N^3)$, but it only requires one-time generation without real-time updates.

V. Fluid Beam Training of RHS-Enabled FAS

This section introduces the fluid beam training scheme for RHS-enabled FAS using sliding windows.

A. Key Idea of the Fluid Beam Training

In conventional beam training based on aperture-fixed arrays, each codeword corresponds to a specific array position. During the comparison of received signal strengths among different codewords, it may occur that some codewords appear at the peaks of the signal envelope depicted in Fig. 6, while others may fall on the troughs due to the small-scale fading. This may potentially lead to errors in the comparison of signal strengths, thereby causing a decrease in the accuracy of beam training.

Benefiting from the aperture-changeable feature of RHS-enabled FAS, multiple array positions can be flexibly selected for codewords with the same beam coverage. By traversing candidate windows, the one yielding the maximum signal strength is selected as the codeword gain. Thus, by utilizing multiple array positions, the probability of the maximum signal strength occurring at envelope troughs can be reduced.

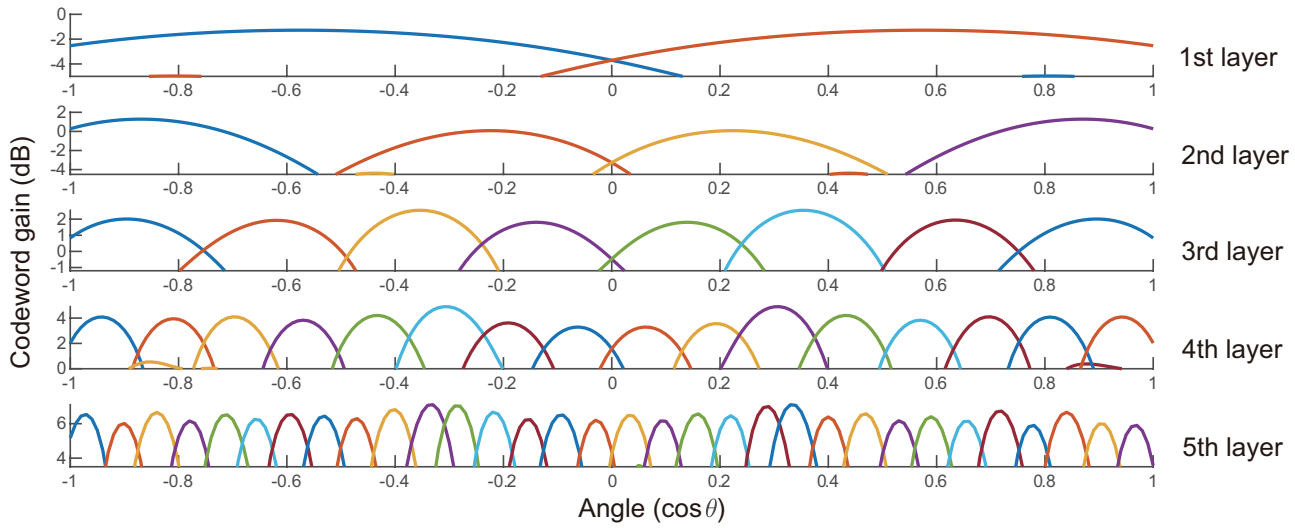

Fig. 9. The beam coverage of codewords at each layer in the RHS hierarchical codebook.

B. Hierarchical Beam Training Using Sliding Windows

As shown in Fig. 8, we use a hierarchical codebook consisting of S layers, each of which contains only two codewords. The beam training is performed layer by layer. For the s-th layer, two codewords are applied for the user to compare the received signal strength. Specifically, each codeword corresponds to multiple sliding windows. We select the Z windows with the highest codeword gain, which corresponds to the sorted codewords $[\mathbf{v}_{s,p,1}, \cdots, \mathbf{v}_{s,p,Z}]$ in **Algorithm** 1. The user then selects the highest signal strength among different windows as the codeword gain of $\mathbf{v}_{s,p}$.

Based on the above sliding window procedure, the user receives multiple signals corresponding to two codewords in the s-th layer. The user compares the signal strengths and feeds back the index 1 or 2 of the codeword with the higher signal strength to the BS. Given the user's feedback τ_s at the s-th layer, the index ξ_s of the optimal codeword at the s-th layer is represented as

$$\xi_s = 2(\xi_{s-1} - 1) + \tau_s, \tag{20}$$

where ξ_0 is set as 1. After obtaining the index of the optimal codeword at the s-th layer, the codeword indices used for beam training at the $(s+1)$-th layer are $2\xi_s - 1$ and $2\xi_s$, respectively. In the bottom layer, the optimal codeword $\mathbf{v}_{S,\xi_S}$ is obtained for the user. The details of the fluid beam training are listed in **Algorithm** 2, which exhibits a computational complexity of $\mathcal{O}(Z \log_2 N)$. The training overhead scales only logarithmically with the number of antennas when extended to large-scale arrays.

C. Performance-Overhead Tradeoff

Defining the overhead of beam training as the number of codewords employed to search for the optimal codeword, the overhead of fluid beam training can be given by $2SZ$, where S is the layer of the codebook and Z is the number of sliding windows for each codeword.

As the number of windows Z increases, the probability of each codeword's signal strength falling into the trough of the signal envelope decreases, thereby enhancing accuracy in codeword selection. However, since the total overhead is directly proportional to the number of utilized windows Z, the overall duration of beam training also increases. Note that the total communication slot ρ comprises the beam training slot ρ_B and the transmission slot ρ_T. The throughput R_E of the system is defined as [36]

$$R_E = \frac{\rho - \rho_B}{\rho} \times R, \tag{21}$$

where R is the data rate. Increasing the number of windows Z for beam training enhances the accuracy of codeword selection, which boosts the data rate R. Meanwhile, this also prolongs the beam training timeslot ρ_B, resulting in a reduced effective transmission $\rho - \rho_B$ given the total timeslot ρ. Therefore, the system throughput can be maximized by adjusting the number of windows.

Remark 3. *An optimal number Z^* of sliding windows exists in fluid beam training, which balances the data rate and effective transmission time to maximize system throughput.*

VI. Simulation Results

In this section, we validate the effectiveness of the proposed RHS codebook design method and fluid beam training scheme based on simulations of a one-dimensional 64-element array and a two-dimensional 4×64-element array, respectively. In the parameter setting, the carrier frequency is set to 26.2 GHz, and the element spacing is $\frac{\lambda}{4}$. The wave number $|\mathbf{k}_s|$ on the RHS surface is $\frac{2\sqrt{3}\pi}{\lambda}$, and the path loss exponent α is 2. The SNR is defined as $\frac{1}{\sigma^2}$, and the number of NLOS paths L is 3.

A. Holographic Patterns of RHS Hierarchical Codebook

Utilizing the codebook design approach in **Algorithm** 1, a 5-layer hierarchical codebook as illustrated in Fig. 9 is designed. Leveraging the amplitude-modulation feature of the RHS, the beamwidth is regulated by adjusting the equivalent aperture of the array. It is observed that the angular coverage

TABLE I
RADIATION CHARACTERISTICS VS. WINDOW POSITION.

Main-lobe amplitude	17.6	17	16.7	16.3	15.9
Main-lobe direction	6 deg.	5 deg.	6 deg.	6 deg.	6 deg.
Side-lobe level (dB)	-7.5	-8.2	-7.8	-8.3	-7.5
Window index	1	2	3	4	5

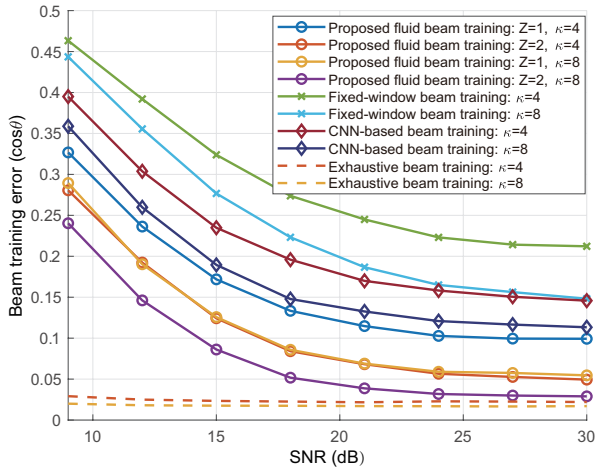

Fig. 10. Beam training error vs. SNR.

of the codewords at each layer aligns with the desired one in Fig. 8, where the beamwidth gradually narrows as the layer number. This validates the effectiveness of the codeword design scheme. Moreover, the codewords at lower layers exhibit higher beam gain, due to more activated RHS elements radiating higher energy.

The influence of window position on beam radiation characteristics for a fixed window size is shown in Table I. Five beams steered in the same direction with different window positions are simulated through CST, where smaller window indices indicate positions closer to the feed. It is observed that mainlobe gain[2], beam direction, and sidelobe levels are stable across various window positions. Beams corresponding to window positions nearer the feed exhibit slightly higher gain due to lower reference wave attenuation.

B. Comparison with Traditional RHS-enabled Beam Training

We compare the proposed fluid beam training scheme with the following RHS-enabled beam training schemes. 1) **Fixed-window based hierarchical beam training**: This approach employs a hierarchical codebook designed using the fixed-position array, which has the same number of codewords as the proposed scheme. There are no sliding windows during beam training. 2) **CNN-based beam training**: This method utilizes a CNN network, which takes the signal strengths of four wide-beam codewords as input and outputs the narrow-beam codeword with the highest selected probability [37]. 3) **Exhaustive beam training**: This method designs a DFT codebook using the entire array, which contains codewords representing all possible angles.

[2]The realized beam gain is determined by the beam directivity, antenna radiation efficiency, and impedance mismatch effects.

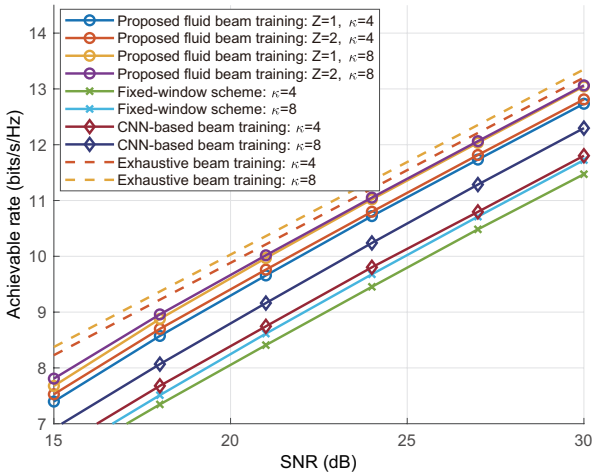

Fig. 11. Achiveable rate vs. SNR.

Fig. 10 shows the variation of beam training error with the SNR for different schemes. Under the same channel conditions, i.e., the Rician factor κ, the error of the proposed sliding-window-based fluid beam training is significantly smaller than that of the fixed-window-based scheme. This illustrates that the degree of freedom in window position can enhance codeword gain, thereby reducing beam training error. The CNN-based approach demonstrates lower beam training error than the fixed-window scheme due to its superior prediction capability, while maintaining lower training overhead compared to the proposed method, since its performance is susceptible to channel condition variations. Increasing the number of windows can further reduce beam training errors, as it improves the channel quality. The beam training error decreases as the SNR increases, and the proposed scheme achieves a training error close to the exhaustive search at high SNR, which serves as a lower bound.

Fig. 11 demonstrates the variation of achievable data rates with the SNR for different schemes. A large Ricean factor κ leads to high data rates, as a high LOS path gain results in strong received signal strength. The proposed fluid beam training scheme using a sliding window exhibits significantly higher data rates compared to the scheme using the fixed window. This suggests that considering the array position could enhance the achievable data rate by improving the codeword gain and channel conditions. Moreover, utilizing more windows during beam training can further improve data rates, as it enhances the channel quality, thereby increasing the received signal strength and avoiding the misselection of codewords.

C. The Impact of the Minimum Amplitude Value of RHS elements

The ideal amplitude range of the RHS spans from $[0, 1]$. However, due to limitations in the element structure, practical RHS elements still radiate energy even when in the off state. Fig. 12 demonstrates the impact of the minimum amplitude value on the performance of fluid beam training.

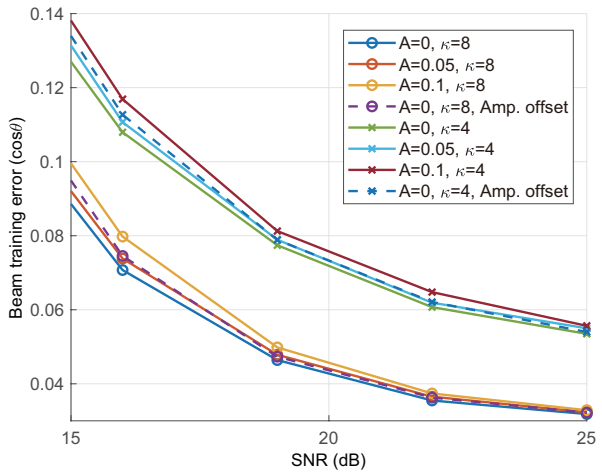

Fig. 12. The impact of the minimum amplitude value and amplitude response offset on beam training error.

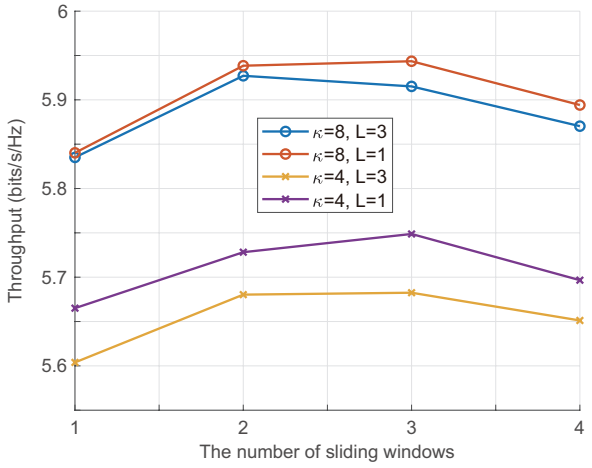

Fig. 13. User throughput vs. the number of sliding windows.

It is observed that under different Rician factors κ, the beam training error is minimized when the minimum amplitude A is 0. This is because fluid beam training requires elements outside the sliding window to be in the absolute off state to accurately control the beamwidth. When $A = 0.05$ and $A = 0.1$, representing elements that still radiate 5% and 10% of the reference wave energy in the off state, respectively, it is found that the beam training error does not increase significantly. This indicates that fluid beam training is effective in practical RHS-enabled FAS. In addition to the minimum amplitude value, the effect of hardware-induced amplitude response offsets on beam training performance is examined. Assuming a 5% random offset between actual and desired element amplitudes, it shows that these amplitude variations increase beam training error due to resulting deviations in the beam pattern. The impact of amplitude offsets on beam training diminishes as SNR increases.

D. Performance-Overhead Tradeoff of Fluid Beam Training

When the SNR = 10 dB, we employ a 4×64-element two-dimensional RHS-enabled FAS to conduct fluid beam training with different numbers of sliding windows. Fig. 13 demonstrates the variation of throughput with the number of sliding windows under different channel conditions. A large Rician factor κ and few NLOS paths could enhance throughput, as the codebook is designed based on the LOS link. The total number of system time slots ρ is set to 800. Under different channel conditions, throughput initially increases and then decreases with the number of windows. There exists an optimal number of windows that balances training overhead and data rate, thereby maximizing throughput, which validates **Remark** 3.

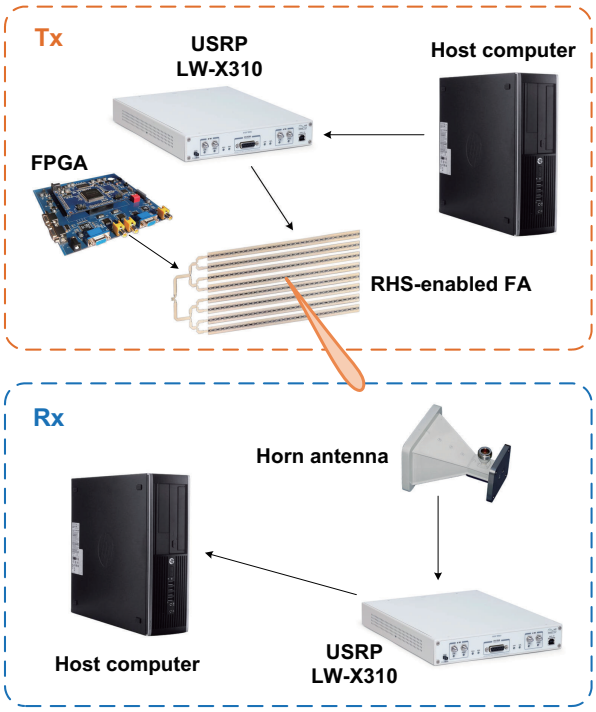

Fig. 14. RHS-enabled FAS based communication platform.

VII. Experimental Results

In this section, we first introduce the RHS-enabled FAS and communication platform. After that, experimental validation is conducted to investigate the signal envelope with different windows of FAS. The proposed fluid beam training scheme is also performed.

A. Implementation of the 384-Element RHS-Enabled FAS

As shown in Fig. 15, the implemented RHS is a two-dimensional array with dimensions of $15.7 \times 9.9 \times 0.123$ cm^3. The RHS comprises 384 elements, arranged in 48 elements per row and 8 elements per column. The feed is positioned at the edge of the metasurface and is connected to a one-to-eight power divider to feed the reference wave into the RHS. The reference wave is guided across the metasurface and propagates toward the other end, exciting each element to radiate energy into free space. The radiation amplitude of each element is controlled by a Field-Programmable Gate Array (FPGA). The FPGA is mounted on the PCB and interfaces with both the individual RHS elements and the host computer. The FPGA incorporates pre-designed software to regulate the bias voltage of the PIN diodes in each element,

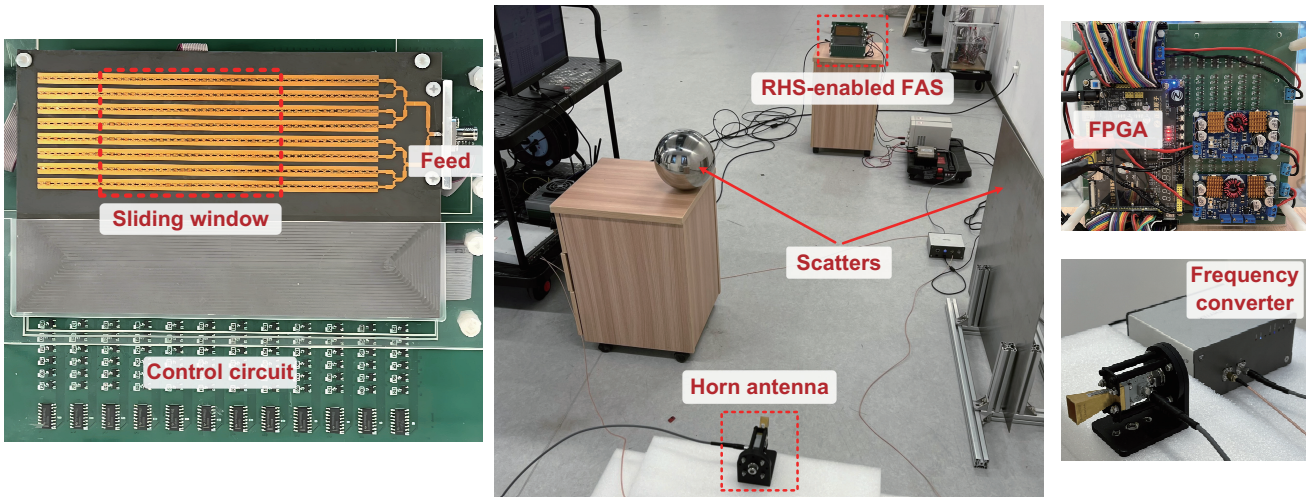

Fig. 15. Implementation of the RHS-enabled FAS based platform.

and the amplitude of the RHS elements varies according to the states of these diodes.

Due to FPGA-controlled element activation method of the RHS, the number and position of activated elements can be altered, making it a viable implementation of fluid antennas. During signal transmission, a series of sliding windows are designed, where the positions of activated elements change according to the window position to enhance the channel quality. Configurations of element amplitudes corresponding to different window sizes and positions, known as codebooks, are pre-stored in the FPGA. in the beam training, switching codewords through the FPGA enables the alteration of element positions.

B. RHS-enabled FAS Communication Platform

Utilizing RHS-enabled FAS, we constructed a communication platform as illustrated in Fig. 14 and 15. The hardware modules of this platform consist of a transmitter (Tx) end and a receiver (Rx) end. In addition to the LOS path, metal scatterers are placed to form NLOS paths. The Tx comprises a host computer, a Universal Software Radio Peripheral (USRP), a frequency converter, and RHS-enabled FAS. The Rx includes a computer, a USRP, a frequency converter, and a horn antenna. The functions of each module are presented below.

- **Transmitter:** A USRP LW-X310 is utilized to generate the baseband signal at Tx, which is capable of achieving RF modulation based on GNU Radio. The signal generated by the USRP is up-converted to 26.2 GHz via a frequency converter, as the maximum operating frequency of the USRP is 6 GHz. The up-converted signal is then fed into RHS-enabled FAS through the feed.
- **Receiver:** The workflow at the Rx is the reverse of that at the Tx. The Rx employs a standard horn antenna (LB-34-10-A) to capture the signals emitted by RHS. The output of the horn antenna is connected to a frequency converter to down-convert the signals to 6 GHz. The down-converted signals are then input into the USRP LW-X310 for RF demodulation and signal processing to recover the original signals.
- **Host computer and FPGA:** The host computers are equipped with a graphical interface for the USRP. In the Tx, parameters such as the transmit power and modulation mode can be controlled, while at the Rx, the received signal strength can be obtained. An FPGA controls the radiation amplitude of each RHS element by adjusting the bias voltage of the diodes. The element amplitude encoding corresponding to the designed codewords is pre-stored in the FPGA, enabling direct retrieval from the host computer during beam training.

C. Signal Envelope Varying with the Sliding Window Position

To verify the variation of received signal strength with the position of the sliding window, i.e., the array position, we designed the following communication experiment. The horn antenna and RHS-enabled FAS are placed at the same height with a horizontal distance of 3.5 m as Fig 15. The horn antenna faced directly towards RHS, located at a horizontal angle of $0°$. Three window sizes of 36×8, 24×8 and 12×8 are designed, offering 13, 25, and 37 possible window positions, respectively. The FPGA is programmed to control each window to generate beams pointing towards $0°$.

Fig. 16 demonstrates the variation of the received SNR with the window position for different window sizes. It is observed that the received SNR varies with the window position for all three window sizes. The differences between the maximum and minimum received SNRs for window lengths of 36, 24, and 12 are 9.92 dB, 10.12 dB, and 13.22 dB, respectively. This indicates that the received signal strength at the user is related to the number of elements within the window. Smaller windows introduce greater randomness in the channel, leading to larger fluctuations in the received SNR, which is consistent with the results presented in Fig. 6. The average received SNR for different window positions across the three window sizes are 14.35 dB, 13.98 dB, and 10.75 dB, respectively, suggesting that large window sizes result in high received SNRs. This is because increasing the number of activated elements enhances both the total radiated energy and the beam directivity.

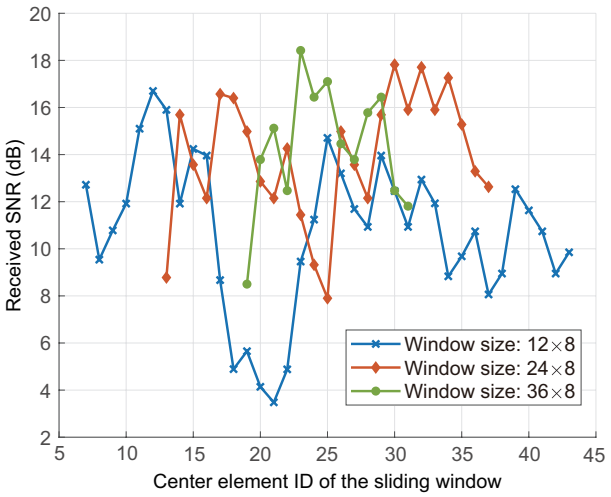

Fig. 16. Received SNR vs. window position under different window sizes.

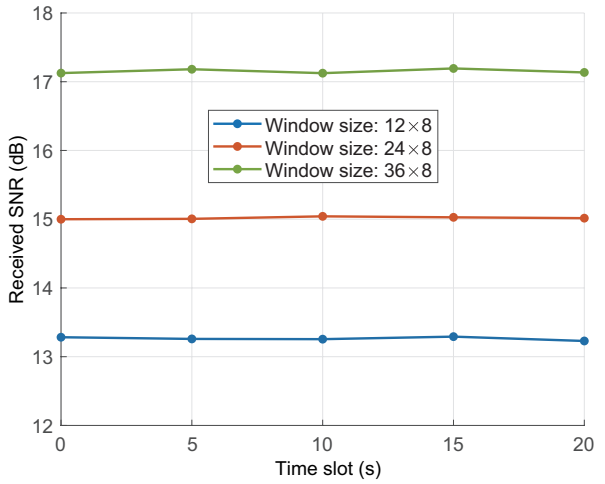

Fig. 17. Received SNR vs. transmission time.

To further validate that the variations in the received signal strength depicted in Fig. 16 can be attributed to changes in the sliding window position rather than temporal variations, we measure the variation of received SNR over time slots at fixed window positions for different window sizes. As shown in Fig. 17, when the window position is fixed, the received SNR exhibits no significant variation over time for all three window sizes. This demonstrates that the primary factor of the change in received SNR is the variation in channel conditions resulting from the sliding of the window position, further validating that optimizing the received SNR could be achieved by adjusting the window position.

D. Fluid Beam Training

Following **Algorithm** 1 and 2, we perform a 5-layer fluid beam training procedure using the RHS-enabled FAS communication platform. Horn antennas are positioned at azimuth angles of $-35°$ and $0°$, respectively. As shown in Fig. 18 and 19, the FPGA controls RHS-enabled FAS to transmit signals starting from the first layer of the codebook. During the beam training, each codeword utilizes two sliding windows for

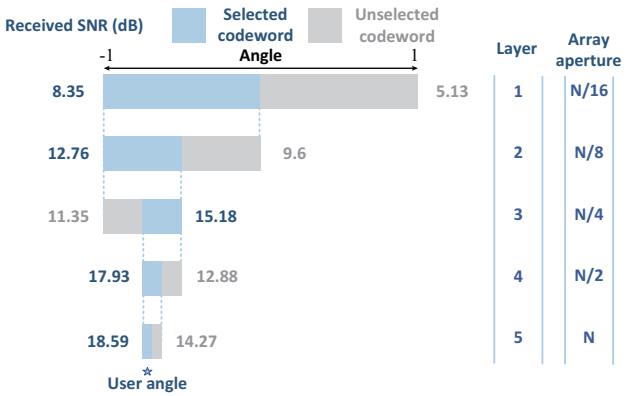

Fig. 18. Fluid beam training: user at $-35°$.

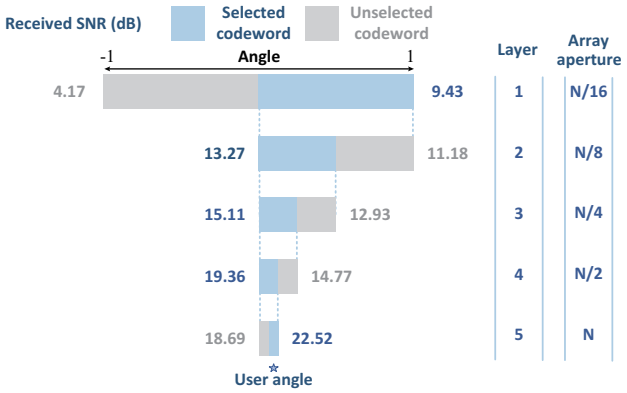

Fig. 19. Fluid beam training: user at $0°$.

signal transmission, and the receiver selects the codeword that maximizes the received SNR. Through layer-by-layer beam training, the size of the sliding windows gradually increases to generate beams with a finer angular resolution, ultimately locking onto the user's angle. The blue codewords in the figures represent the selected codewords at each layer. It is observed that the user angles in both directions are successfully acquired at the bottom layer, validating the feasibility of the proposed fluid beam training.

In practical deployments, RHS-enabled FAS may encounter challenges related to high-frequency switching speed requirements for element reconfiguration and robustness in harsh operational environments [38], which we will investigate in our future work.

VIII. Conclusions

In this paper, we propose a fluid antenna system implemented by RHS to perform codebook design and beam training based transmission. We reveal that the equivalent aperture and position of the array can be reconfigured via element-wise amplitude modulation. Considering the mutual coupling of radiated energy between RHS elements, a hierarchical codebook is first designed, where the angular coverage of codewords narrows progressively layer by layer, achieved by adjusting the equivalent aperture of RHS. Based on these multi-resolution codewords, we then propose a fluid beam training scheme, where each codeword corresponds to multiple sliding windows to enhance channel quality. A 384-element

RHS-enabled FAS communication platform is implemented to conduct beam training experiments.

Both simulation and experiment results demonstrate that: 1) By adjusting the equivalent aperture of the RHS array through amplitude modulation, codewords with different angular coverage can be generated using only 1-bit amplitude modulation. Hierarchical beam training employing these codewords can accurately obtain the user angle. 2) The received signal strength varies with the sliding window position of RHS-enabled FAS. By adjusting the window position, the channel quality can be improved to enhance the received signal strength. 3) Compared to beam training using the fixed window position, beam training based on the sliding window yields smaller training errors and higher data rates. There also exists an optimal number of windows that maximizes the throughput.

REFERENCES

[1] D. Zhou, M. Sheng, J. Li and Z. Han, "Aerospace Integrated Networks Innovation for Empowering 6G: A Survey and Future Challenges," *IEEE Commun. Surv. Tutorials*, vol. 25, no. 2, pp. 975-1019, Secondquarter 2023.

[2] C. You *et al.*, "Next Generation Advanced Transceiver Technologies for 6G and Beyond," *IEEE J. Sel. Areas Commun.*, vol. 43, no. 3, pp. 582-627, March 2025.

[3] L. Bai, Z. Huang, Y. Ge, R. Yu, L. Wang and X. Cheng, "Cellular Vehicle-to-Everything (C-V2X) Testing: From Theory to Practice," *IEEE Network*, *early access*, DOI: 10.1109/MNET.2025.3534196.

[4] K. -K. Wong, A. Shojaeifard, K. -F. Tong and Y. Zhang, "Fluid Antenna Systems," *IEEE Trans. Wireless Commun.*, vol. 20, no. 3, pp. 1950-1962, March 2021.

[5] K. -K. Wong and K. -F. Tong, "Fluid Antenna Multiple Access," *IEEE Trans. Wireless Commun.*, vol. 21, no. 7, pp. 4801-4815, July 2022.

[6] W. K. New, K. -K. Wong, H. Xu, K. -F. Tong, C. -B. Chae and Y. Zhang, "Fluid Antenna System Enhancing Orthogonal and Non-Orthogonal Multiple Access," *IEEE Commun. Lett.*, vol. 28, no. 1, pp. 218-222, Jan. 2024.

[7] K. -F. Tong, B. Liu, and K. -K. Wong, "Designs and Challenges in Fluid Antenna System Hardware," *Electronics*, vol. 14, no. 7, p. 1458, 2025.

[8] L. Zhu, W. Ma and R. Zhang, "Movable Antennas for Wireless Communication: Opportunities and Challenges," *IEEE Commun. Mag.*, vol. 62, no. 6, pp. 114-120, June 2024.

[9] J. Zhang *et al.*, "A Novel Pixel-Based Reconfigurable Antenna Applied in Fluid Antenna Systems With High Switching Speed," *IEEE Open J. Antennas Propag.*, vol. 6, no. 1, pp. 212-228, Feb. 2025.

[10] B. Liu, K. -F. Tong, K. -K. Wong, C. -B. Chae, and H. Wong, "Be Water, My Antennas: Riding on Radio Wave Fluctuation in Nature for Spatial Multiplexing using Programmable Meta-Fluid Antenna," *arXiv preprint*, arXiv:2502.04693, 2025.

[11] D. Zhang, S. Ye, M. Xiao, K. Wang, M. Di Renzo and M. Skoglund, "Fluid Antenna Array Enhanced Over-the-Air Computation,"*IEEE Wireless Commun. Lett.*, vol. 13, no. 6, pp. 1541-1545, June 2024.

[12] C. Wang, Z. Li, K. -K. Wong, R. Murch, C. -B. Chae and S. Jin, "AI-Empowered Fluid Antenna Systems: Opportunities, Challenges, and Future Directions," *IEEE Wireless Commun.*, vol. 31, no. 5, pp. 34-41, October 2024.

[13] W. K. New, K. -K. Wong, H. Xu, K. -F. Tong and C. -B. Chae, "Fluid Antenna System: New Insights on Outage Probability and Diversity Gain," *IEEE Trans. Wireless Commun.*, vol. 23, no. 1, pp. 128-140, Jan. 2024.

[14] Sungjoon Lim, C. Caloz and T. Itoh, "Metamaterial-Based Electronically Controlled Transmission-Line Structure as a Novel Leaky-Wave Antenna with Tunable Radiation Angle and Beamwidth," *IEEE Trans. Microwave Theory Tech.*, vol. 52, no. 12, pp. 2678-2690, Dec. 2004.

[15] R. Deng *et al.*, "Reconfigurable Holographic Surfaces for Ultra-Massive MIMO in 6G: Practical Design, Optimization and Implementation," *IEEE J. Sel. Areas Commun.*, vol. 41, no. 8, pp. 2367-2379, Aug. 2023.

[16] Y. Gao, H. Vinck and T. Kaiser, "Massive MIMO Antenna Selection: Switching Architectures, Capacity Bounds, and Optimal Antenna Selection Algorithms," *IEEE Trans. Signal Process.*, vol. 66, no. 5, pp. 1346-1360, 1 March1, 2018.

[17] Z. Zhang, J. Zhu, L. Dai and R. W. Heath, "Successive Bayesian Reconstructor for Channel Estimation in Fluid Antenna Systems," *IEEE Trans. Wireless Commun.*, vol. 24, no. 3, pp. 1992-2006, March 2025.

[18] S. Zhang, Y. Zhang and B. Di, "Large-Scale Intelligent Surfaces Enabled Unified Near-Field and Far-Field Communications: Codebook Design and Beam Training," *IEEE Network*, vol. 39, no. 1, pp. 90-96, Jan. 2025.

[19] J. An et al., "Codebook-Based Solutions for Reconfigurable Intelligent Surfaces and Their Open Challenges," *IEEE Wireless Commun.*, vol. 31, no. 2, pp. 134-141, April 2024.

[20] Y. Chen, M. Chen, H. Xu, Z. Yang, K. -K. Wong and Z. Zhang,"Joint Beamforming and Antenna Design for Near-Field Fluid Antenna System," *IEEE Wireless Commun. Lett.*, vol. 14, no. 2, pp. 415-419, Feb. 2025.

[21] L. Zhou, J. Yao, T. Wu, M. Jin, C. Yuen and F. Adachi, "Fluid Antenna-Assisted Simultaneous Wireless Information and Power Transfer Systems," *IEEE Trans. Veh. Technol.*, vol. 74, no. 5, pp. 8285-8290, May 2025.

[22] W. K. New *et al.*, "A Tutorial on Fluid Antenna System for 6G Networks: Encompassing Communication Theory, Optimization Methods and Hardware Designs," *IEEE Commun. Surveys Tuts*, *early access*, DOI: 10.1109/COMST.2024.3498855.

[23] W. K. New, K. -K. Wong, H. Xu, F. Rostami Ghadi, R. Murch and C. -B. Chae, "Channel Estimation and Reconstruction in Fluid Antenna System: Oversampling is Essential," *IEEE Trans. Wireless Commun.*, vol. 24, no. 1, pp. 309-322, Jan. 2025.

[24] H. Xu et al., "Channel Estimation for FAS-Assisted Multiuser mmWave Systems," *IEEE Wireless Commun. Lett.*, vol. 28, no. 3, pp. 632-636, March 2024.

[25] C. Skouroumounis and I. Krikidis, "Fluid antenna with linear MMSE channel estimation for large-scale cellular networks," *IEEE Trans. Commun.*, vol. 71, no. 2, pp. 1112–1125, Feb. 2023.

[26] R. Deng, B. Di, H. Zhang, Y. Tan and L. Song, "Reconfigurable Holographic Surface-Enabled Multi-User Wireless Communications: Amplitude-Controlled Holographic Beamforming," *IEEE Trans. Wireless Commun.*, vol. 21, no. 8, pp. 6003-6017, Aug. 2022.

[27] X. Zhang, H. Zhang, L. Liu, Z. Han, H. V. Poor and B. Di, "Target Detection and Positioning Aided by Reconfigurable Surfaces: Reflective or Holographic?," *IEEE Trans. Wireless Commun.*, vol. 23, no. 12, pp. 19215-19230, Dec. 2024.

[28] S. Zhang, B. Di, A. Kaushik and Y. C. Eldar, "Holographic-Pattern Based Multi-User Beam Training in RHS-Aided Hybrid Near-Field and Far-Field Communications," *IEEE Trans. Wireless Commun.*, *early access*, DOI: 10.1109/TWC.2025.3569654.

[29] L. Bai, Z. Huang, J. Liu, L. Cui, M. Sheng and X. Cheng, "A Mixed-Bouncing Based 6G Multi-UAV Integrated Channel Model With Consistency and Non-Stationarity," *IEEE Trans. Wireless Commun.*, vol. 23, no. 10, pp. 13456-13470, Oct. 2024.

[30] S. Hu, H. Wang and M. C. Ilter, "Design of Near-Field Beamforming for Large Intelligent Surfaces," *IEEE Trans. Wireless Commun.*, vol. 23, no. 1, pp. 762-774, Jan. 2024.

[31] Y. Liu, Z. Wang, J. Xu, C. Ouyang, X. Mu and R. Schober, "Near-Field Communications: A Tutorial Review," *IEEE Open J. Commun. Soc.*, vol. 4, pp. 1999-2049, 2023.

[32] A. M. Elbir, A. Abdallah, A. Celik and A. M. Eltawil, "Antenna Selection With Beam Squint Compensation for Integrated Sensing and Communications," *IEEE J. Sel. Top. Signal Process.*, vol. 18, no. 5, pp. 857-870, July 2024.

[33] C. A. Balanis, Antenna Theory: Analysis and Design. Hoboken, NJ, USA: Wiley, 2016, pp. 285–351.

[34] Y. Lu, Z. Zhang and L. Dai, "Hierarchical Beam Training for Extremely Large-Scale MIMO: From Far-Field to Near-Field," *IEEE Trans. Commun.*, vol. 72, no. 4, pp. 2247-2259, April 2024.

[35] B. Di, H. Zhang, Z. Han, R. Zhang and L. Song, "Reconfigurable Holographic Surface: A New Paradigm for Ultra-Massive MIMO," *IEEE Trans. Cognit. Commun. Networking*, *early access*, DOI: 10.1109/TCCN.2025.3547043.

[36] S. Zhang, Y. Zhang, H. Zhang, N. Ye and B. Di, "Rate-Overhead Tradeoff for IOS-Aided Beam Training: How Large Codebook Is Enough for the IOS?," *IEEE Wireless Commun. Lett.*, vol. 12, no. 6, pp. 1081-1085, June 2023.

[37] K. Ma, D. He, H. Sun, Z. Wang and S. Chen, "Deep Learning Assisted Calibrated Beam Training for Millimeter-Wave Communication Systems," *IEEE Trans. Commun.*, vol. 69, no. 10, pp. 6706-6721, Oct. 2021.

[38] B. Di, S. Zhang, Z. Han and R. Zhang, "Holographic Beamforming with Leakage Power Constraints," *IEEE Wireless Commun.*, vol. 32, no. 4, pp. 14-21, August 2025.